BREAKUP OF ^{12,14}Be ON PROTON TARGET AT INTERMEDIATE ENERGIES: EVIDENCE OF THE d-WAVE DOMINANCE INSIDE ^{12}Be

L. X. Chung[1], C. A. Bertulani[3], Oleg A. Kiselev[2], D. T. Khoa[1] and Peter Egelhof[2]

[1]Institute for Nuclear Science and Technology, VINATOM, 179 Hoang Quoc Viet, Cau Giay, Hanoi, Vietnam

[2] GSI Helmholtzzentrum für Schwerionenforschung, D-64291 Darmstadt, Germany

[3] Department of Physics and Astronomy, Texas A & M University-Commerce, Commerce, TX 75429, USA

Abstract: The transverse momentum distribution of ^{11,12}Be from the breakup of ^{12,14}Be on a proton target at 700.5, and 700 MeV/u, respectively, have been measured. The ground state configuration of ^{12}Be was studied within the framework of the distorted wave impulse approximation (DWIA) using quasi-free scattering assumption (QFS). The result shows the existence of a $d\frac{5}{2}^+$ single-particle state with the spectroscopic factor of 2.73(30) in ^{12}Be which is interpreted as evidence for an intruder state in this nucleus.

1 Introduction

Many studies of halo nuclei have been carried out by measuring interaction cross sections $\sigma_{\rm I}$ [1], reaction cross sections $\sigma_{\rm R}$ [2], angular differential cross sections of nucleus-proton elastic scattering [3–6] or fragment's momentum distributions [7–9]. Among them, the last mentioned method is efficient to probe the ground state configuration of halo nuclei [8, 9], which can be a mixture of several configurations and the shape of the momentum distribution relates to the angular momentum of valence neutrons [10].

The structures of ^{12,14}Be are of particular interest since they belong to the $N = 8$ isotones which is a magic number in the shell model's point of view. They are halo nuclei [5, 11] with a large asymmetry of neutron and proton numbers which leads to the disapearance of the $N = 8$ shell closure [12–14]. This magic state is dependent on proton number. For instance, the $N = 8$ state intrudes in ^{12}Be but not in ^{14}C, and in ^{32}Mg but not in ^{34}Si. When the proton $j_>$ orbital is full, the neutron number is magic. If the orbital lacks of protons, the neutron number of the full $j_<$ orbital is no longer magic, and the next shell intrudes [12]. In this paper we present the experimental momentum distributions of ^{11,12}Be fragments from ^{12}Be(p,pn)^{11}Be and ^{14}Be(p,$p2n$)^{12}Be reactions at $\approx$ 700 MeV/u measured at GSI Darmstadt. The structure of ^{12}Be was studied by using the DWIA and QFS for the single nucleon knockout reaction [15].

Barker [13] first pointed out the existence of a $d\frac{5}{2}^+$ intruder state in ^{12}Be. After that, the ground state of ^{12}Be was observed to intrude first by Navin *et al.* [14] from the analysis of the ^{9}B(^{12}Be,^{11}Be+γ) reaction at 78 MeV/u. They concluded that a mixture of s- and p-wave in the ground state of ^{12}Be exists, and suggested the existence of a d-wave which was not seen because the $d\frac{5}{2}^+$ state of ^{11}Be decays via neutron emission, not detected by their experiment. Following the suggestion in Ref. [14], a ^{12}C(^{12}Be,n^{11}Be) experiment was performed to check the $d\frac{5}{2}^+$ state [12], and the result concluded its significant existence.

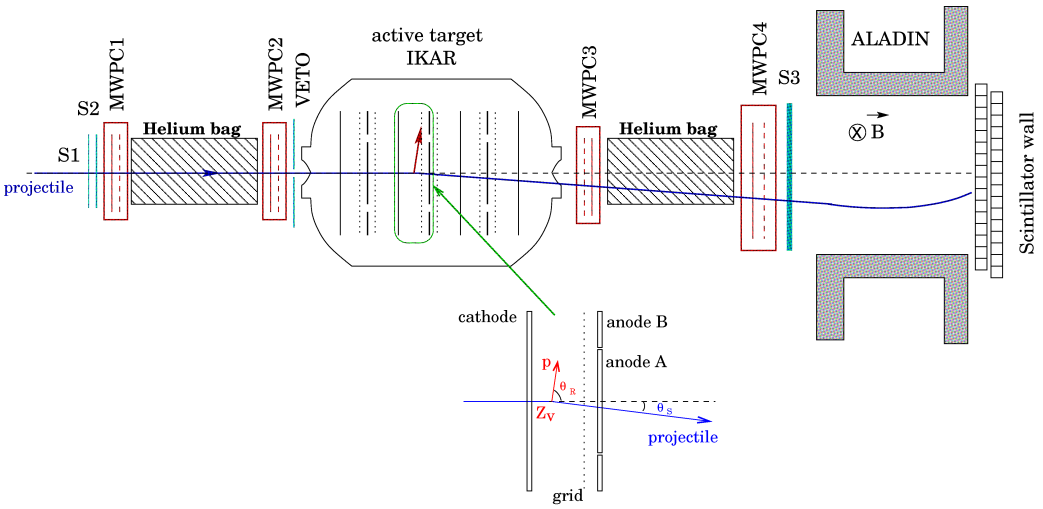

FIGURE 1: Schematic view of the experimental setup. The main part is the IKAR ionization chamber serving as an active target. The 4 multi-wire proportional chambers MWPC1-MWPC4 were used for beam and projectile tracking to determine the scattering angles. The helium bags were used to reduce the projectile interaction with matter. The scintillators S1-S3 and VETO were used for beam identification and triggering. The ALADIN magnet and the position sensitive scintillator wall were used for the fragment identification. This figure is taken from Ref. [5].

In the present study, we report an evidence for the dominance of the d-wave inside ^{12}Be ground state from the analysis of the breakup data of ^{12}Be on a proton target.

2 Experiment

The experimental setup was described in details in Ref. [5]. A primary ^{18}O beam produced at the MEVVA (MEtal Vapour Vacuum Arc) source was accelerated to about 750 MeV/u energy by the UNILAC (UNiversal Linear ACelerator) and the heavy-ion synchrotron (SIS) at GSI Darmstadt. Afterwards, the beam was focused on an 8 g/cm^2 beryllium production target at the entrance of the FRagment Separator (FRS) [16]. The beryllium ions produced by fragmentation of ^{18}O nuclei were separated by the FRS according to their magnetic rigidity. The energies of the secondary beams ^{12,14}Be were 700.5, and 700 MeV/u, respectively. They were transported to the target cave where the experimental setup was installed (Fig. 1). The main part of the setup was the ionization chamber IKAR [17–20], which served simultaneously as a gas target and a recoil proton detector. IKAR was filled with hydrogen gas and operated at 10 bar pressure [5]. The recoil signal was measured in coincidence with the scattered ^{12,14}Be particles.

2.1 Projectile identification

The projectile identification was done by the energy loss and time of flight (ToF) methods. The energy losses were measured by detectors S1, S2 and S3, and their signals were also

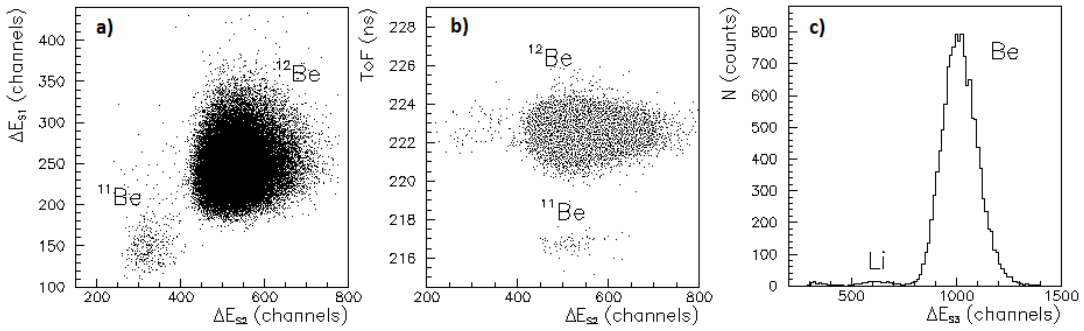

FIGURE 2: The selection of the ^{12}Be beam. Panel a) displays the correlation between energy loss in S1 and S2, $\Delta E_{\rm S1}$ vs. $\Delta E_{\rm S2}$. The correlation of the time of flight and the energy loss in S2, ToF vs. $\Delta E_{\rm S2}$, is presented in panel b). The energy loss in S3 $\Delta E_{\rm S3}$ is plotted in panel c) to select the isotope of a certain Z.

used for triggering. The ToF was measured by the scintillation detector S8 (not shown in Fig. 1), placed at the end of the FRS and S1. The flight path was 40 m and the ToF for the Be isotope was typically 223 ns. The circular-aperture scintillator VETO selected the projectiles which entered IKAR within an area of 2 cm in diameter around the central axis.

Figures 2 illustrates the selection of the ^{12}Be beam. The beam selection was done by a proper cut condition on panels a) and b) to select the ^{12}Be projectiles and the Be peak in panel c) to make sure that beryllium isotopes were chosen after the reaction. A similar figure can be found in Ref. [5] for the case of ^{14}Be. The contaminants were determined to be about 1.1 %, and 25 % [5] in the case of ^{12,14}Be beams, respectively. Most of the contaminants in the ^{12}Be beam were ^{11}Be, while most of the contaminants in the ^{14}Be beam were ^{11}Li.

2.2 Breakup event selection and the fragment's transverse momentum distribution

After the selection of the beam, the reaction channel was selected with the identification of the fragment. This procedure was done by using the ALADIN magnet and the scintillator wall (see Fig. 1). First, the correlation between the position on the scintillator wall and the scattering angle in the x-plane of the reaction product, $x_{\rm wall}$ vs. $\theta_{\rm x}$, was plotted to select ^{11,12}Be events as presented in panels a) and b) in Fig. 3. Then, the selection for the Be peak detected by the scintillator wall in Fig. 3.c was added to assure the nuclear charge of the selected events.

The scattering angle θ_s of the fragment was measured by a tracking system consisting of 2 pairs of two-dimensional multi-wire proportional chambers (PC1-PC2 and PC3-PC4), arranged upstream and downstream with respect to IKAR. At very low momentum transfer, the scattering angle is calculated as

$$\theta_s = \sqrt{\theta_x^2 + \theta_y^2} \tag{1}$$

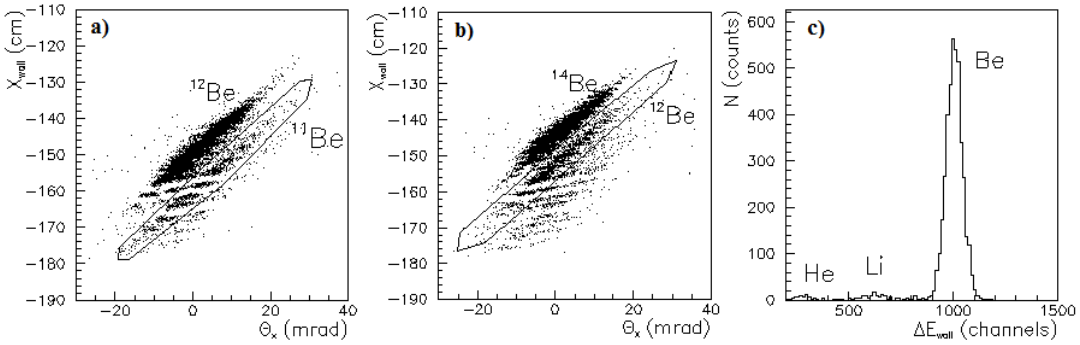

FIGURE 3: Identification for ^{11,12}Be fragments. Panels a) and b) present the correlation between the position on the scintillator wall and the scattering angle in x-plane of the residue, $x_{\rm wall}$ vs. $\theta_{\rm x}$ used to select the fragments. Panel c) presents the energy spectrum of the scintillator wall used to confirm the residual nuclear charge.

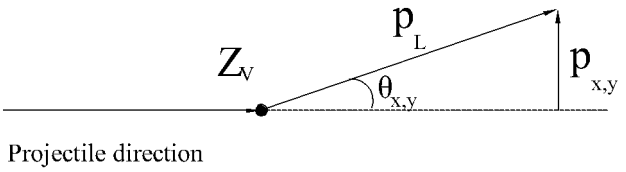

FIGURE 4: Relation between the transverse momentum ($p_{x(y)}$) and total momentum ($p_{\rm L}$) of the fragment .

where, $\theta_{x(y)}$ were measured by PC1-PC4. The scattering angular resolution measured by the MWPCs was estimated by a run without target to be $\sigma_{\rm x} = 0.61$ mrad [5].

At high energy, the interaction of the projectile with the target participants happens so quickly that almost making no perturbation on the other nucleons (adiabatic approximation). The non participating nucleons in the target can be considered as "spectators" [21] which scatter elastically off the target. Following this idea, in the current problem, the clusters ^{11,12}Be inside the halo nuclei ^{12,14}Be were considered as the spectators. Therefore, the elastic scattering kinematics of ^{11,12}Be+p were applied to determine the momenta of ^{11,12}Be fragments, where, the scattering angles $\theta_{\rm s}$ were measured as discussed above, and the velocity of the clusters were assumed to be equal to those of the projectiles.

At very low momentum transfer, the x and y projections of the transverse momentum of the fragment (see Fig. 4) are calculated as

$$p_{\rm x,y} = p_{\rm L} \sin(\theta_{\rm x,y}), \tag{2}$$

where, $p_{\rm L}$ is the momentum of the fragment in the laboratory frame.

The differential cross section was determined according to the experimental data from the breakup event number dN in an interval dp_x using the following formula

$$\frac{{\rm d}\sigma}{{\rm d}p_x} = \frac{{\rm d}N}{{\rm d}p_x.M.n_{\rm t}.\Delta L}, \tag{3}$$

where, M is the number of incident projectiles, $n_{\rm t}$ the target density known from the

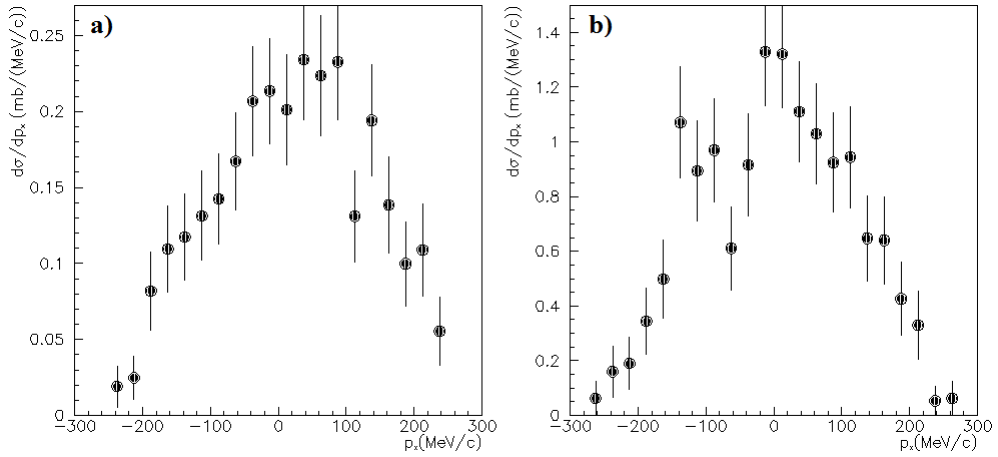

FIGURE 5: Transverse momentum distributions of the fragments ^{11,12}Be. Panel a) displays the case of ^{11}Be after the ^{12}Be(p,pn)^{11}Be reaction at $E = 700.5$ MeV/u. Panel b) displays the case of ^{12}Be after the ^{14}Be(p,$p2n$)^{12}Be reaction at $E = 700$ MeV/u. The errors are statistical.

measured H_2 gas pressure and temperature, ΔL the effective target thickness. Figure 5 a) and b) present the deduced transverse momentum distributions of ^{11,12}Be fragments after the p(^{12}Be, ^{11}Be) and p(^{14}Be, ^{12}Be) reactions at energies of 700.5, and 700 MeV/u, respectively.

3 Distorted wave impulse approximation for single-nucleon knockout reaction

The distorted wave impulse approximation (DWIA) is known as an efficient approach to treat the single-nucleon knockout reaction [15, 22, 23]. The difficulty of this reaction is that there are three particles emerging in the exit channel whose exactly kinematical calculation does not exist. Therefore, the formalism is based on quasifree scattering (QFS) assumption at high energy (100-1000 MeV/u).

3.1 Quasifree scattering

The transition amplitude for $A(p,pN)B$ reaction is

$$T_{p,pN} = \sqrt{S(lj)}\langle\Psi_f|\tau_{p\to pN}(\boldsymbol{r}'_{pB},\boldsymbol{r}'_{NB};\boldsymbol{r}_{pA},\boldsymbol{r}_{NB})|\Psi_i\rangle, \quad (4)$$

where, $N = p, n$, Ψ_i and Ψ_f are the initial and final states of the system, $\sqrt{S(lj)}$ is the corresponding spectroscopic factor for a bound nucleon N inside the target $A = N+B$ with quantum number jl, $\tau_{p\to pN}$ is the scattering matrix being dependent on the interaction of pA through radius $\boldsymbol{r}_{pA}$ and NB through radius $\boldsymbol{r}_{NB}$ in the initial channel, and of pB through radius $\boldsymbol{r}'_{pB}$ and NB through radius $\boldsymbol{r}'_{NB}$ in the final channel.

The QFS assumes that the interaction between p and N is dominant. In the entrance channel, B is considered as a spectator. In other words, the range of the pN interaction is so much smaller than the nuclear size that reduces the scattering matrix to

$$\tau_{p\to pN}(\boldsymbol{r}'_{pB}, \boldsymbol{r}'_{NB}; \boldsymbol{r}_{pA}, \boldsymbol{r}_{NB}) \approx \tau_{p\to pN}(\boldsymbol{r}'_{pN}; \boldsymbol{r}_{pN}). \tag{5}$$

Using the Fourier transformation, the pN scattering matrix can be written to be dependent on the momentum $\boldsymbol{k}$ as $\tau_{p\to pN}(\boldsymbol{k}'_{pN}, \boldsymbol{k}_{pN}; E)$ with E being the scattering energy. Prime sign implies the quantity in the exit channel.

3.2 Distorted wave impulse approximation

The scattering amplitude is factorized in the DWIA using the QFS as [15, 22]

$$\begin{aligned} T_{p,pN} &= \sqrt{S(lj)}\langle\Psi_f|\tau_{p\to pN}(\boldsymbol{k}'_{pN}, \boldsymbol{k}_{pN}; E)|\Psi_i\rangle \\ &= \sqrt{S(lj)}\langle\chi^{(-)}_{\boldsymbol{k}'_p}\chi^{(-)}_{\boldsymbol{k}'_N}|\tau_{p\to pN}(\boldsymbol{k}'_{pN}, \boldsymbol{k}_{pN}; E)|\chi^{(+)}_{\boldsymbol{k}_p}\psi_{jlm}\rangle, \end{aligned} \tag{6}$$

where, $\chi^{(-)}_{\boldsymbol{k}'_p}$ ($\chi^{(-)}_{\boldsymbol{k}'_N}$) denotes the distorted wave for an outgoing (knocked-out nucleon) in the presence of the residual nucleus B, $\chi^{(+)}_{\boldsymbol{k}_p}$ is the distorted wave for an incoming proton in the presence of the target nucleus A, and ψ_{jlm} is the bound state of the knocked-out nucleon. These two-body distorted wave are not dependent on the presence of the others according to the impulse approximation.

At high energy, the above distorted waves are determined by using the eikonal approximation

$$\chi^{(\pm)} = S_{(\pm)} \exp(i\boldsymbol{k}^{(\pm)}.\boldsymbol{r}), \tag{7}$$

where, S matrix is calculated with given optical interaction potentials [15]. "+" and "-" signs stand for "in" and "out", respectively. One possible choice of the optical potential is with direct and imaginary parts to be the M3Y [24] and the $t-\rho\rho$ [25] potentials, respectively,

$$U_{\rm opt}(\boldsymbol{r}) = U^{\rm M3Y}(\boldsymbol{r}) + U_{\rm C}(\boldsymbol{r}) - i\frac{E}{k}\sigma(E)\int \rho_{A(B)}(\boldsymbol{r}-\boldsymbol{r}')\rho_N(\boldsymbol{r}')\mathrm{d}^3r'. \tag{8}$$

In the above equation, $U_{\rm C}$ is the Coulomb potential between pA in the entrance channel, or between pB or NB in the exit channel. $\rho_{A(B)}$ is the density of the nucleus $A(B)$. ρ_N is the intrinsic matter density of proton or neutron whose energy and momentum are denoted by E and k, respectively. $\sigma(E)$ is the nucleon-nucleon cross section at energy E.

The knocked-out nucleon bound state wave function ψ_{jlm} is decoupled into angular and radial parts as [15]

$$\psi_{jlm}(\mathrm{r}) = \frac{u_{lj}(r)}{r}\sum_{m_l,m_s}\langle lm_l sm_s|jm\rangle Y_{lm_l}(\hat{r})\chi_{m_s}, \tag{9}$$

where, $\boldsymbol{j} = \boldsymbol{l} + \boldsymbol{s}$ with l and s being the angular momentum and intrinsic spin, m and $m_{l(s)}$ are the projection of $\boldsymbol{j}$ and $\boldsymbol{l(s)}$, χ_{m_s} is the spinor wavefunction, and $\langle lm_l sm_s|jm\rangle$ is the Clebsch-Gordan coefficient. Y is a spherical harmonic function. The radial part $u_{lj}(r)$ is normally determined from a Wood-Sacxon potential with the parameters being adjusted so that the state binding energy E_{lj} is reproduced. In the case of ^{12}Be, to reproduce -3.17 (MeV) [14] binding energy of the $s\frac{1}{2}^+$ state, the parameters of the nuclear and spin-orbit potentials are chosen to be $U_0 = -66.201$ (MeV), $r_0 = 2.747$ (fm), $a_0 = 0.65$ (fm), and $U_{\rm S0} = -10.0$ (MeV), $r_{\rm S0} = 2.747$ (fm) and $a_{\rm S0} = 0.65$ (fm). In which, U, r and a denote the depth, radius and diffuseness of the Wood-Sacxon potential.

3.3 Transverse momentum distribution

We rewrite the two-body wave function for incoming and outgoing channels as

$$\begin{aligned} \Psi_{\rm in} &= S_{\rm in} \exp(i\alpha \boldsymbol{k}_p \boldsymbol{r}) \psi_{jlm} && (10) \\ \Psi_{\rm out} &= S^{(p)}_{\rm out} S^{(N)}_{\rm out} \exp\left[i(\boldsymbol{k}'_p + \boldsymbol{k}_N \right] && (11) \end{aligned}$$

where, $S_{\rm in}$, $S^{(p)}_{\rm out}$ and $S^{(N)}_{\rm out}$ are scattering matrices for pA in the entrance channel, pB and NB in the exit channel, respectively. $\alpha = \dfrac{A-1}{A}$ is the correction for the center of mass motion [15, 22]. The scattering transition is calculated as

$$\begin{aligned} T_{p,pN} &= \sqrt{S(lj)} \langle \Psi_{\rm out} | \tau_{p\to pN}(\boldsymbol{k}'_{pN}, \boldsymbol{k}_{pN}; E) | \Psi_{\rm in} \rangle && (12) \\ &= \sqrt{S(lj)} \tau_{p\to pN}(\boldsymbol{k}'_{pN}, \boldsymbol{k}_{pN}; E) \int {\rm d}^3 r e^{-i\boldsymbol{p}.r} S(b,\theta) \psi_{jlm}(r). \end{aligned}$$

In these above equations, $\theta = \theta(\theta'_p, \theta_N)$ is a function of outgoing angles θ'_p and θ_N, and

$$S(b,\theta) = S_{pA}(E_p, b) S_{p'B}(E'_p, \theta'_p, b) S_{NB}(E_N, \theta_N, b), \quad (13)$$

with the momentum transfer defined as

$$\boldsymbol{p} = \boldsymbol{k}'_p + \boldsymbol{k}_N - \alpha \boldsymbol{k}_p. \quad (14)$$

This value is a modification of the missing momentum $\boldsymbol{Q}$ satisfied the on-shell conservation:

$$\begin{aligned} \epsilon &= E_N + E'_p - E_p - m_N \\ \boldsymbol{Q} &= \boldsymbol{k}'_p + \boldsymbol{k}_N - \boldsymbol{k}_p, && (15) \end{aligned}$$

where, m_N is the nucleon mass, ϵ is the missing energy [15].

The differential scattering cross section for the reaction $A(p,pN)B$ by knocking out a nucleon from the orbital jl under the conditions of fixed $\boldsymbol{p}$ is determined in the DWIA

using the QFS as [15]

$$\frac{\mathrm{d}\sigma_{lj}}{\mathrm{d}^3p} = \frac{1}{(2\pi)^3}\frac{S(lj)}{2j+1}\sum_m \langle\frac{\mathrm{d}\sigma_{pN}}{\mathrm{d}\Omega}\rangle_p \times \mid\int \mathrm{d}^3r e^{-i\boldsymbol{p}.r}\langle S(b,\theta)\rangle_p\psi_{jlm}(r)|^2. \quad (16)$$

$\langle\frac{\mathrm{d}\sigma_{pN}}{\mathrm{d}\Omega}\rangle$ and the scattering matrices are averaged over all possible energies of the final proton and nucleon, the later are also averaged over all pp' scattering angles. In which, all used cases lead to the same magnitude of the momentum transfer p. The longitudinal and transverse components of $\boldsymbol{p}$ are denoted as $\boldsymbol{p}_z$ and $\boldsymbol{p}_t$, respectively, then $\boldsymbol{p} = \boldsymbol{p}_z + \boldsymbol{p}_t$. The transverse momentum distribution is the product when we integrate over p_z the function in the right hand side of Eq. (16) [15]

$$\frac{\mathrm{d}\sigma_{lj}}{\mathrm{d}^2p_t} = \frac{S(lj)}{2\pi(2j+1)}\sum_m \langle\frac{\mathrm{d}\sigma_{pN}}{\mathrm{d}\Omega}\rangle_{p_t}|C_{lm}|^2 \int_{-\infty}^{\infty} dz \times \mid\int_0^{\infty} db\langle S(b)\rangle_{p_t}\frac{u_{lj}(r)}{r}J_m(p_tb)P_{lm}(b,z)|^2, \quad (17)$$

where, J_m are cylindrical Bessel functions, P_{lm} are the Legendre polynomials. The distribution of the x-component of the transverse momentum is calculated as [26]

$$\frac{\mathrm{d}\sigma_{lj}}{\mathrm{d}p_\mathrm{x}} = \int \mathrm{d}p_\mathrm{y}\frac{\mathrm{d}\sigma_{lj}}{\mathrm{d}^2p_t}(p_\mathrm{x},p_\mathrm{y}), \quad (18)$$

Eq. (18) the is calculation of the differential cross section for one nucleon knockout at a given jl bound state, so called exclusive differential cross section. The total (inclusive) differential cross sections is equal to the sum over all possible jl. One can write

$$\frac{\mathrm{d}\sigma}{\mathrm{d}p_\mathrm{x}} = \sum_{lj} S(lj)\frac{\mathrm{d}\sigma_{lj}}{\mathrm{d}p_\mathrm{x}}. \quad (19)$$

As discussed above, $\boldsymbol{p}$ is a modification of the missing momentum $\boldsymbol{Q}$ to correct for the c.m motion. Thus, Eq. (19) presents the momentum distribution of the residual core B after the (p,pN) reaction.

4 Result of the analysis for ^{12}Be$(p,pn)^{11}$Be

^{12}Be was assumed to compose of a ^{11}Be core and a valence neutron. The calculated differential $x-$transverse momentum cross sections of the ^{12}Be$(p,pn)^{11}$Be reaction corresponding to three single particle states $s\frac{1}{2}^+$, $p\frac{1}{2}^-$ and $d\frac{5}{2}^+$ of the valence neutron according to Eq. (18) is presented in FIG. 6 left. The spectroscopic factors of these states were set

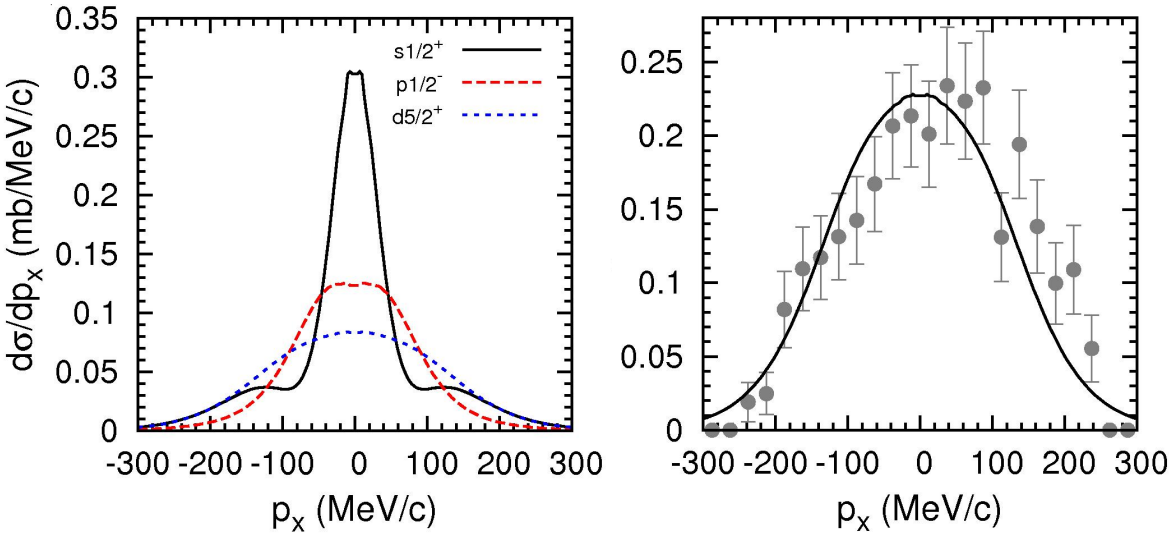

FIGURE 6: The calculated differential $x-$transverse momentum cross sections (spectroscopic factor being equal to 1) of the ^{12}Be$(p,pn)^{11}$Be reaction corresponding to three single particle states $s\frac{1}{2}^+$ (solid), $p\frac{1}{2}^-$ (dashed) and $d\frac{5}{2}^+$ (dots) are shown on the left. The experimental data (points) are fitted by the $d5/2^+$ calculated cross sections (solid line) with the spectroscopic factor $S(d\frac{5}{2}^+)$ of 2.73(30) (right).

to 1. The calculated cross sections were used to fit the experimental data on FIG. 5.a according to Eq. (19). The best-fit result is displayed in FIG. 6 right which leads to a spectroscopic factor of 2.73(30) for only $d\frac{5}{2}^+$ bound state of ^{12}Be. The result gives an evidence that a neutron of the $l = 2$ orbital was knocked out in the $p(^{12}$Be,^{11}Be) reaction at 700.5 MeV/u, and the $d-$wave is dominant in the ground state of ^{12}Be. This demonstrates the intruder state at $N = 8$ in this nucleus, in agreement with the conclusions in Refs. [12–14].

In conclusion, the transverse momentum distribution of the residues after the breakup reactions is a good tool to study the structure of the mother nuclei. At high energy (from several hundreds of keV), the "spectator" assumption is suitable which can be applied to simplify the kinematics of the breakup reactions to the elastic scattering of the cluster inside the projectile and the target. The experimental data of the transverse momentum distribution of ^{11,12}Be from the breakups of ^{12,14}Be on a proton target at 700.5, and 700 MeV/u, respectively, were measured. The analysis of the ^{11}Be data by using DWIA gives an evidence in the dominant existence of the d-wave in ^{12}Be which shows the breakdown of the $N = 8$ magic number in ^{12}Be. Using the same procedure to analyse the data from ^{14}Be$(p,p2n)^{12}$Be the structure of ^{14}Be can be study but one needs the theoretical calculation.

References

[1] I. Tanihata, H. Hamagaki, O. Hashimoto, Y. Shida, and N. Yoshikawa, *Physical Review Letters* **55**, (1985) 2676.

[2] M. Fukuda, T. Ichihara, N. Inabe, T. Kubo, H. Kumagai, T. Nakagawa, Y. Yano, I. Tanihata, *Physics Letters B* **268**, (1991) 339.

[3] P. Egelhof, *Prog. Part. Nucl. Phys.* **46**, (2001) 307.

[4] G.D. Alkhazov *et al.*, *Nuclear Physics A* **712**, (2002) 269.

[5] S. Ilieva *et al.*, *Nuclear Physics A* **875**, (2012) 8.

[6] Le Xuan Chung, Oleg A. Kiselev, Dao T. Khoa, and Peter Egelhof, *Physical Review C* **92**, (2015) 034608.

[7] M. Zhar *et al.*, *Physical Review C* **48**, (1993) R1484.

[8] T. Kobayashi, O. Yamakawa, K. Omata, K. Sugimoto, T. Shimoda, N. Takahashi and I. Tanihata, *Physical Review Letters* **60**, (1988) 2599.

[9] Y. Kondo *et al.*, *Physics Letters B* **690**, (2010) 245.

[10] I. Tanihata, H. Savajols, and R. Kanungo, *Progress in Particle and Nuclear Physics* **68**, (2013) 215.

[11] M. Labiche *et al.*, *Physical Review Letters* **86**, (2001) 600.

[12] S.D. Pain *et al.*, *Physical Review Letters* **96**, (2006) 032502.

[13] F.C. Barker, *Journal of Physics G* **2**, (1976) L45.

[14] A. Navin *et al.*, *Physical Review Letters* **85**, (2000) 266.

[15] T. Aumann, C. A. Bertulani and J. Ryckebusch, *Physical Review C* **88** 064610, (2013) pp. 1-15.

[16] H. Geissel *et al.*, Nucl. Instrum. Methods **B70**, (1992) 286.

[17] A.A. Vorobyov, G.A. Korolev, V.A. Schegelsky, G.YE. Solyakin, G.L. Sokolov and YU.K. Zalite, *Nuclear Instruments and Methods* **119**, (1974) 509.

[18] G.D. Alkhazov *et al.*, Phys. Rev. Lett. **78**, (1997) 2313.

[19] S.R. Neumaier *et al.*, *Nuclear Physics A* **712**, (2002) 247.

[20] A.V. Dobrovolsky *et al.*, *Nuclear Physics A* **766**, (2006) 1.

[21] M.S. Hussein and K.W. McVoy, *Nuclear Physics A* **124**, (1985) 139.

[22] Gerhard Jacob and Th. A. J. Maris (1966), *Reviews of Modern Physics* **38** 121.

[23] T. Udagawa, A. Schulte and F. Osterfeld,*Nuclear Physics A* **474** (1987) 131.

[24] G. Bertsch, J. Borysowicz, H. McManus, and W. G. Love, *Nuclear Physics A* **284**, (1977) 399.

[25] M.S. Hussein, R.A. Rego and C.A. Bertulani, *Physics Reports* **201**, (1991) 279.

[26] C. A. Bertulani and A. Gade, *Comp. Phys. Comm.* **175**, (2006) 372.